A shallow-water equation based one-dimensional dynamic wave model with non-hydrostatic pressure

Wei, Z.; Jia, Y.

Coastal wave is one of major forces that dominate coastal hydronydamics, sediment transport, morphology and threaten coastal infrastructures. In recent years, the non-hydrostatic technique for solving Reynolds-averaged Navier-Stokes equations has been developed for wave propagation study. It has been shown that this method has a comparable accuracy for wave simulation to Boussinesq-type approaches and a better computing efficiency.

In this paper, a one-dimensional depth-integrated non-hydrostatic pressure wave model for wave propagation, breaking and run-up is developed based on the numerical method proposed by Stelling and Duinmeijer. In this numerical method, the non-conservative form of Navier-Stokes equation is solved for either momentum conservation or energy head conservation by applying different advection approximation methods. The method is, therefore, able to handle rapidly varied water flows (such as wave breaking) in wide range of Froude numbers. When wave run-up is concerned, wetting and drying treatment plays a key role for many numerical models. The wet & dry handling approach in the method is simple, efficient and capable of reserving positive water depth.

In this non-hydrostatic wave model development, the fractional time step method is adopted. The shallow water equations without non-hydrostatic pressure terms are solved for approximation of velocity; a tri-diagonal equation for non-hydrostatic pressure terms is then solved, and the approximate velocity is corrected by non-hydrostatic pressure terms. The free surface elevation is calculated by the depth-averaged continuity equation to satisfy global mass conservation. This model will be validated by an analytical solution and several benchmark wave dynamics test cases; it is anticipated the model can predict wave breaking and run-up processes effectively.

INTRODUCTION

In recent years, numerical simulations of wave motions using the non-hydrostatic pressure methods (Casulli and Stelling, 1998; Stansby and Zhou, 1998) have advanced a lot. Stelling and Zijlema (2003) improved the efficiency and accuracy of non-hydrostatic method by utilizing an edge-based compact difference scheme for the approximation of vertical gradient of the non-hydrostatic pressure located at the interface between vertical layers, with correct implementation of zero pressure boundary at the water surface, their model obtained good agreements with the linear dispersion relation with only two layers. Subsequent efforts were made

to improve the model's efficiency, stability, and capability of handling wave breaking and run-up (Zijlema and Stelling, 2005, 2008); recently, an operational public domain code: SWASH was released (Zijlema et al., 2011). Following them, several non-hydrostatic models, for example, depth-averaged models (Walters, 2005; Yamazaki et al., 2008; Cui et al., 2012), two-layer models (Bai and Cheung, 2011, 2012) and multi-layer models (Ai et al., 2011; Ai and Jin, 2012; Ma et al., 2012) have been developed.

In order to properly simulate discontinuous flows, such as hydraulic jump and wave breaking, the numerical models should conserve the momentum

A Shallow-Water Equation Based One-Dimensional Dynamic Wave Model with Non-Hydrostatic Pressure
Wei, Jia

(Stelling and Duinmeijer, 2003). In general, two strategies have been used to achieve momentum conservation in the numerical formulation. In case that the non-conservative form of governing equations is under consideration, a momentum conservation scheme proposed by Stelling and Duinmeijer (2003) can be used to handle wave breaking (Yamazaki et al., 2008; Zijlema et al., 2011). The other way is to solve the conservation form of governing equations directly, since the momentum conservation is automatically considered, this method has also been widely used for wave breaking simulation (Zijlema and Stelling, 2008; Ai and Jin, 2012; Ma et al., 2012).

After a wave breaks, a portion of the remaining energy will energize a bore that will run up the face of a beach or sloped shore structure (Sorensen, 2006). In the numerical model, use of a moving boundary condition is required for the calculation of wave run-up and run-down. The detailed reviews on wetting and drying algorithms for coastal waves run-up modeling can be found at Zijlema and Stelling (2008).

In this paper, a one-dimensional depth-integrated non-hydrostatic wave model for wave propagation, breaking and run-up is developed. Non-hydrostatic approach is introduced into an existing shallow water model (Stelling and Duinmeijer, 2003), which solves the non-conservation form of shallow water equations with a momentum conservation scheme for handling hydraulic jumps and uses a simple wetting and drying algorithm for simulating the moving boundary. The newly developed non-hydrostatic model is able to simulate wave propagation, breaking and run-up. The paper is organized as follows. The governing equations and associated boundary conditions are introduced in Section 2. Section 3 describes the numerical solution. Section 4 presents an analytical solution and several benchmark cases for model verification and validation. Finally, conclusions are drawn in Section 5.

MATHEMATICAL FORMULATION
Governing equations
The three-dimensional Reynolds-averaged Navier-Stokes equations are given by

$$\frac{\partial u}{\partial x} + \frac{\partial v}{\partial y} + \frac{\partial w}{\partial z} = 0 \tag{1}$$

$$\frac{\partial u}{\partial t} + \frac{\partial(uu)}{\partial x} + \frac{\partial(uv)}{\partial y} + \frac{\partial(uw)}{\partial z} = -\frac{1}{\rho}\frac{\partial p}{\partial x} + \frac{1}{\rho}\frac{\partial \tau_{xx}}{\partial x} + \frac{1}{\rho}\frac{\partial \tau_{xy}}{\partial y} + \frac{1}{\rho}\frac{\partial \tau_{xz}}{\partial z} \tag{2}$$

$$\frac{\partial v}{\partial t} + \frac{\partial(vu)}{\partial x} + \frac{\partial(vv)}{\partial y} + \frac{\partial(vw)}{\partial z} = -\frac{1}{\rho}\frac{\partial p}{\partial y} + \frac{1}{\rho}\frac{\partial \tau_{yx}}{\partial x} + \frac{1}{\rho}\frac{\partial \tau_{yy}}{\partial y} + \frac{1}{\rho}\frac{\partial \tau_{yz}}{\partial z} \tag{3}$$

$$\frac{\partial w}{\partial t} + \frac{\partial(wu)}{\partial x} + \frac{\partial(wv)}{\partial y} + \frac{\partial(ww)}{\partial z} = -g - \frac{1}{\rho}\frac{\partial p}{\partial z} + \frac{1}{\rho}\frac{\partial \tau_{zx}}{\partial x} + \frac{1}{\rho}\frac{\partial \tau_{zy}}{\partial y} + \frac{1}{\rho}\frac{\partial \tau_{zz}}{\partial z} \tag{4}$$

where u, v, w are flow velocities in x, y, z directions, respectively; t is time, ρ is water density; p is the pressure; g is the gravitational acceleration, τ_{xx}, τ_{xy} ..., and τ_{zz} are the stresses (including both molecular and turbulent effects).

Following Casulli and Stelling (1998) and Stelling and Zijlema (2003), the total pressure is split into hydrostatic and non-hydrostatic parts as

$$p = \rho g(\eta - z) + \hat{q} \tag{5}$$

where $\eta(x, y, t)$ is the free surface elevation, $\zeta(x, y)$ is the bed elevation, and the total water depth is $H = (\eta(x,y,t) - \zeta(x,y))$. The vertical datum is arbitrary, but it is usually set equal to the still water level (sea level) for coastal and oceanographic researches as shown in Figure 1.

The free surface and bottom kinematic boundary conditions are

$$w_\eta = \frac{D\eta}{Dt} = \frac{\partial \eta}{\partial t} + u_\eta \frac{\partial \eta}{\partial x} + v_\eta \frac{\partial \eta}{\partial y} \qquad \text{at } z = \eta \tag{6}$$

$$w_\zeta = \frac{D\zeta}{Dt} = u_\zeta \frac{\partial \zeta}{\partial x} + v_\zeta \frac{\partial \zeta}{\partial y} \qquad \text{at } z = \zeta \tag{7}$$

Depth integration of Equations (1)-(4) from to by taking into account the pressure in Equation (5) and the boundary conditions of Equations (7) and (8), ignoring the viscosity term, and following the non-hydrostatic pressure term treatments of Stelling and Zijlema (2003) and Walters (2005). The governing equations in Cartesian coordinate system are derived as

$$\frac{\partial \eta}{\partial t} + \frac{\partial(HU)}{\partial x} = 0 \tag{8}$$

$$\frac{\partial U}{\partial t} + U\frac{\partial U}{\partial x} = -g\frac{\partial \eta}{\partial x} - \frac{gn^2 U|U|}{H^{4/3}} - \frac{1}{2\rho H}\left(H\frac{\partial q}{\partial x} + q\left(\frac{\partial \eta}{\partial x} + \frac{\partial \zeta}{\partial x}\right)\right) \tag{9}$$

$$\frac{\partial W}{\partial t} = \frac{q}{\rho H} \tag{10}$$

where U, W are depth-integrated velocities in horizontal and vertical directions, respectively; q is the non-hydrostatic pressure at the bottom and n is the Manning coefficient. As the distribution of vertical velocity is unknown, it is approximated by $W = (w_\zeta + w_\eta) / 2$. Due to introduction of the non-hydrostatic pressure and incompressibility (Casulli and Stelling, 1998; Stelling and Zijlema, 2003), the above equations are solved together with the two-dimensional vertical form of continuity equation (1):

$$\frac{\partial u}{\partial x} + \frac{\partial w}{\partial z} = 0 \qquad (11)$$

Boundary conditions
To obtain a unique solution, boundary conditions are required at all the boundaries of the physical domain considered. At the free surface, since the current model doesn't consider the wind stress and surface tension, the atmospheric pressure boundary condition is used.

At the bottom, Manning equation is used to approximate the bed friction, and the vertical velocity at the bed surface is prescribed by the bottom kinematic boundary condition (7).

At the inlet, an incident normal velocity is given based on the linear wave theory as

$$u_I = \frac{\omega f_r}{k(\eta_I - \zeta)} \eta_I \qquad (12)$$

where $\omega = 2\pi/L$ is the angular frequency of wave with T the wave period; $\kappa = 2\pi/L$ is the wave number with L the wave length; η_I is the incident wave surface elevation, for a regular wave, it is usually specified as a sinusoidal or monochromatic wave; f_I is a ramp function used to prevent initially short waves with relatively large amplitudes (Stelling and Zijlema, 2003) and it is defined as

$$f_r(t) = \frac{1}{2}(1 + \tanh\frac{t - 3T}{T}) \qquad (13)$$

The non-hydrostatic pressure is implicitly assumed as zero at inlet.

At the outlet and both ends of solitary wave cases, the flow is assumed hydrostatic. To allow the waves to cross the outflow boundary without reflections,

Sommerfeld's radiation boundary condition is applied:

$$\frac{\partial f}{\partial x} + c\frac{\partial f}{\partial x} = 0 \qquad (14)$$

where f can be water surface elevation and velocity, c is the phase velocity defined as $c = \sqrt{gH}$.

Numerical Formulation
In this research, the governing equations are discretized based on a one-dimensional grid $\{x_{i-1/2} | x_{i+1/2} = i\Delta x, i=0, ..., M\}$ with M the number of grid cells and Δx the length of the grid cell. The location of the cell center is given by $x_i = (x_{i-1/2} + x_{i+1/2}) / 2$. A staggered grid convention is used in which velocity U is located at $x_{i+1/2}$ on the other hand, free surface elevation η and the other variables $\zeta, w_\eta, w\zeta$ and H are located at x_i.

The governing equations are solved semi-implicitly with several steps. In the first step, the momentum equation without non-hydrostatic pressure terms is explicitly solved for the provisional velocity; in the second step, a tri-diagonal equation for non-hydrostatic pressure is constructed using the continuity equation (11) and implicitly solved, and then the provisional velocity is updated; finally, the water depth is updated by solving the depth-integrated continuity equation to ensure global mass conservation.

First step
In this step, the provisional velocity is calculated by the momentum equation (9) without the non-hydrostatic pressure terms as

$$\frac{\partial U}{\partial t} + U\frac{\partial U}{\partial x} + g\frac{\partial \eta}{\partial x} + \frac{gn^2 U|U|}{H^{4/3}} = 0 \qquad (15)$$

and it is discretized as

$$\frac{\bar{U}_{i+1/2}^{n+1} - U_{i+1/2}^n}{\Delta t} + ADV + g\frac{\eta_{i+1}^n - \eta_i^n}{\Delta x} + \frac{n^2 g U_{i+1/2}^{n+1}|U_{i+1/2}^n|}{(\bar{H}_{i+1/2}^{4/3})^n} = 0 \qquad (16)$$

where $U_{i+1/2}^n$ is the horizontal velocity at previous time level, $\bar{H}_{i+1/2}^n$ the water depth at a velocity point, is averaged from the neighboring water depths at surface points. ADV is the discretization of the advective term, and it is approximated by a momentum conservation scheme proposed by Stel-

A Shallow-Water Equation Based One-Dimensional Dynamic Wave Model with Non-Hydrostatic Pressure
Wei, Jia

ling and Duinmeijer (2003) as

$$ADV = \left(u\frac{\partial u}{\partial x}\right)_{i+1/2}^{n} = \max(u_{\rightarrow},0)\left(\frac{u_{i+1/2}^{n}-u_{i-1/2}^{n}}{\Delta x}\right)+\min(u_{\leftarrow},0)\left(\frac{u_{i+3/2}^{n}-u_{i+1/2}^{n}}{\Delta x}\right) \quad (17)$$

with

$$u_{\rightarrow} = \frac{\bar{q}_{i}^{n}}{\bar{H}_{i+1/2}^{n}}, \ u_{\leftarrow} = \frac{\bar{q}_{i+1}^{n}}{\bar{H}_{i+1/2}^{n}}, \ \bar{q}_{i}^{n} = \frac{q_{i+3/2}^{n}+q_{i+1/2}^{n}}{2} \text{ and } q_{i+1/2}^{n} = \hat{H}_{i+1/2}^{n}U_{i+1/2}^{n}.$$

The water depth at a velocity point $\hat{H}_{i+1/2}^{n}$ is simply calculated by a first-order upwind scheme as follows:

$$\hat{H}_{i+1/2}^{n} = \begin{cases} H_{i}^{n}, & \text{if } U_{i+1/2}^{n} > 0 \\ H_{i+1}^{n}, & \text{if } U_{i+1/2}^{n} < 0 \\ \max(\eta_{i}^{n},\eta_{i+1}^{n})-\max(\varsigma_{i}^{n},\varsigma_{i+1}^{n}), & \text{if } U_{i+1/2}^{n} = 0 \end{cases} \quad (18)$$

Second step
In the second step, to achieve a divergence-free velocity field, a tri-diagonal equation is formulated using continuity equation, the momentum equation and bottom kinematic boundary condition and it is implicitly solved for non-hydrostatic pressure. And then the provisional velocity field is corrected by non-hydrostatic pressure.

The vertical velocity at the bottom is calculated by Equation (6) as

$$w_{\varsigma i}^{n+1} = \bar{\bar{U}}_{i}^{n}\frac{\varsigma_{i+3/2}-\varsigma_{i+1/2}}{\Delta x} \quad (19)$$

where $\bar{\bar{U}}_{i}^{n}$, the horizontal velocity at surface points, is calculated by $\bar{\bar{U}}_{i}^{n} = \left(\tilde{U}_{i-1/2}^{n}+\tilde{U}_{i+1/2}^{n}\right)/2$.

The vertical velocity at the free surface is calculated by vertical momentum equation (10) with the approximation $W = (w_{\varsigma} + w_{\eta}) / 2$ and therefore,

$$w_{\eta i}^{n+1} = w_{\eta i}^{n} - w_{\varsigma i}^{n+1} + w_{\varsigma i}^{n} + \frac{2\Delta t q^{n+1}}{\rho H_{i}^{n}} \quad (20)$$

Comparing Equation (15) with Equation (9), it is seen that the final horizontal velocity influenced by the non-hydrostatic pressure can be written as

$$\frac{U_{i+1/2}^{n+1}-\tilde{U}_{i+1/2}^{n+1}}{\Delta t} + \frac{1}{2\rho}\frac{q_{i+1}^{n+1}-q_{i}^{n+1}}{\Delta x} + \frac{1}{2}\frac{\bar{q}_{i+1/2}^{n+1}}{\rho\bar{H}_{i+1/2}^{n}}\frac{(\eta_{i+1}^{n}+\varsigma_{i+1})-(\eta_{i}^{n}+\varsigma_{i})}{\Delta x} = 0 \quad (21)$$

The non-hydrostatic pressure is calculated using the discretized continuity equation (11) as follows

$$\frac{U_{i+1/2}^{n+1}-U_{i-1/2}^{n+1}}{\Delta x} + \frac{w_{\eta i}^{n+1}-w_{\varsigma i}^{n+1}}{H_{i}^{n}} = 0 \quad (22)$$

Substituting Equations (19), (20) and (21) into Equation (22), a tri-diagonal equation for non-hydrostatic pressure is obtained:

$$A_W q_{i-1}^{n+1} + A_P q_{i}^{n+1} + A_E q_{i+1}^{n+1} = S \quad (23)$$

where

$$A_W = \frac{\Delta t}{4\rho}\frac{((\eta_i^n+\varsigma_i)-(\eta_{i-1}^n+\varsigma_{i-1}))}{\bar{H}_{i-1/2}^n\Delta x^2} - \frac{\Delta t}{2\rho\Delta x^2}$$

$$A_P = \frac{\Delta t}{\rho\Delta x^2} + \frac{2\Delta t}{\rho(H_i^n)^2} + \frac{\Delta t}{4\rho}\frac{((\eta_i^n+\varsigma_i)-(\eta_{i-1}^n+\varsigma_{i-1}))}{\bar{H}_{i-1/2}^n\Delta x^2} - \frac{\Delta t}{4\rho}\frac{((\eta_{i+1}^n+\varsigma_{i+1})-(\eta_i^n+\varsigma_i))}{\bar{H}_{i+1/2}^n\Delta x^2}$$

$$A_E = -\frac{\Delta t}{4\rho}\frac{((\eta_{i+1}^n+\varsigma_{i+1})-(\eta_i^n+\varsigma_i))}{\bar{H}_{i+1/2}^n\Delta x^2} - \frac{\Delta t}{2\rho\Delta x^2}$$

$$S = 2\bar{U}_i^n\frac{\varsigma_{i+3/2}-\varsigma_{i+1/2}}{H_i^n\Delta x} - \frac{\tilde{U}_{i+1/2}^{n+1}-\tilde{U}_{i-1/2}^{n+1}}{\Delta x} - \frac{w_{\eta i}^n+w_{\varsigma i}^n}{H_i^n}$$

Equation (23) can be efficiently solved by a tri-diagonal solver (e.g. TDMA). Once the non-hydrostatic pressure is obtained, the horizontal velocity is corrected by Equation (21), and the vertical velocity at the free surface is updated by Equation (20).

Third step
In the last step, the depth-integrated continuity equation (8) is solved for the water depth using the corrected horizontal velocity as

$$\frac{\eta_i^{n+1}-\eta_i^n}{\Delta t} + \frac{\hat{H}_{i+1/2}^n U_{i+1/2}^{n+1}-\hat{H}_{i-1/2}^n U_{i-1/2}^{n+1}}{\Delta x} = 0 \quad (24)$$

In case that the bed is fixed, Equation (24) can be rewritten as

$$\frac{H_i^{n+1}-H_i^n}{\Delta t} + \frac{\hat{H}_{i+1/2}^n U_{i+1/2}^{n+1}-\hat{H}_{i-1/2}^n U_{i-1/2}^{n+1}}{\Delta x} = 0 \quad (25)$$

In Stelling and Duinmeijer (2003), a simple and efficient wetting and drying algorithm was proposed to obtain the non-negative depth with a semi-implicit formulation, and their algorithm is adopted for explicit time integration in this study. It is assumed that the velocity is positive, with the water depth at a velocity point $\hat{H}_{i+1/2}^n$ defined in Equation (17), Equation (25) is rearranged to be

$$H_i^{n+1} = H_i^n(1-\frac{\Delta t}{\Delta x}U_{i+1/2}^n) + H_{i-1}^n U_{i-1/2}^n \quad (26)$$

and therefore, the total water depth is ensured to be positive if . Similar requirement can be derived for a negative flow velocity.

MODEL VERIFICATION AND VALIDATION
In this section, the developed one-dimensional dynamic wave model is verified by an analytical solution and validated by three benchmark cases for nearshore phenomena simulation.

Solitary wave propagation along a constant water depth channel

The solitary wave is a nonlinear wave with finite amplitude, which is not a solution of the hydrostatic shallow water equations, and therefore it is first used to verify the correctness of the non-hydrostatic model. If the fluid is inviscid and the horizontal bottom is frictionless, the wave should maintain the shape and velocity during the propagation process. This case has been used in several non-hydrostatic model verifications (Stelling and Zijlema, 2003; Zijlema and Stelling, 2005; Walters, 2005; and Yamazaki et al., 2008). In this numerical test, a 1000 m long and 10 m deep frictionless channel with radiation boundary condition imposed at both ends is considered. The initial solitary wave is located at x_0=100 m and its initial height is A=2m. The mesh size is Δx=0.5 m, the time step is Δt=0.025 s, and the Courant number in terms of wave celerity is Cr =

$$= \Delta t \sqrt{gH} / \Delta x \approx 0.5.$$

Figure 2 shows the initial solitary wave and simulated wave along the channel at 20, 40 and 60 s. There is a slight reduction of wave height at the beginning of simulation due to the initial condition approximated by the analytical solution, similar observations were reported by Walters (2005) and Yamazaki et al. (2008). It can be seen that the shape and amplitude are conserved well during the simulation, this is attributed to the non-hydrostatic pressure terms in the formulation.

Regular waves propagation over a submerged bar

The second numerical test investigates the wave model's capability to handle nonlinear dispersive waves propagation. Beji and Battjes (1993) and Luth et al. (1994) conducted physical experiments of regular waves propagation over a submerged trapezoidal bar in a 37.7 m long, 0.8 m wide and 0.75 m high wave flume. Figure 3 shows the numerical setup of the experiment, the still water depth is 0.4 m, a 0.3 m bar with offshore slope 1:20 and shoreward slope 1:10 is set between 6.0 m and 17.0 m in the flume. The incident sinusoidal waves with amplitude 1.0 cm and wave period 2.02 s, corresponding to the wave depth parameter $kH \approx 0.67$,

are generated at left side. The wave absorber of the experiment, a 1:25 plane beach with coarse material at the right side, is modeled by an open flow area with the radiation boundary condition imposed (Stelling and Zijlema, 2003; Yamazaki et al., 2008). Surface elevations were measured with wave gauges at several locations. In the simulation, the 35 m long computational domain is discretized with Δx = 1.25 cm, and time step Δt = 0.0025 s.

Comparison of simulated and measured free surface elevations is shown in Figure 4. It is seen that the wave shoaling process on the offshore side of bar (Gauges 4 and 5) and wave transformation from a low frequency dispersion zone (Gauge 6) to a high frequency dispersion zone (Gauge 8) are well predicted by this depth-integrated non-hydrostatic model. However, obvious discrepancies appear between simulated and measured water surface elevations over the flat bottom behind the bar, in this area, the highly dispersive waves with water depth parameters range from 6 to 10 in this zone (Roeber et al., 2010), are out of the applicable range of depth-integrated model. However, these high dispersive waves have been simulated very well by a multi-layer non-hydrostatic model (Stelling and Zijlema, 2003).

Solitary wave run-up along a plane beach

The third numerical test examines the model's capability to handle wave breaking and wave run-up. Titov and Synolakis (1995) presented a solitary wave with wave height A/h = 0.3 (h is the still water depth) ran up a beach with slope 1:19.85. In the numerical model setup, the grid size is $\Delta x/h$=0.125, Manning coefficient n = 0.01 is used to define the surface roughness, and the initial solitary wave is at 20h from the beach toe. Figure 5 compares the simulated surface profiles with the measurement. As the wave propagates over the sloped beach, the wave front starts to skew, and eventually the wave breaks between $t\sqrt{g/h}$=20 and $t\sqrt{g/h}$=25, the numerical model successfully simulates the wave breaking process without any stability issues. And then the breaking water surges over the beach and a hydraulic jump forms around $t\sqrt{g/h}$=50. Overall,

the numerical model reasonably predicts the wave run-up, a minor discrepancy is observed for the location of the return flow around $t\sqrt{g/h}=55$ this was also reported in other numerical test (Yamazaki et al., 2008; Roeber et al., 2010).

Solitary wave propagation over a fringing reef
The last case is a solitary wave transformation over an idealized fringing reef, validating the model's capability in handling nonlinear dispersive waves and wave bore propagation. Two series of laboratory experiments on solitary waves transformation over idealized fringing reefs at the O.H. Hinsdale Wave Research Laboratory of Oregon State University were reported by Roeber et al. (2010). In this study, the considered test involves a solitary wave of wave height A = 0.5 m in a 48.8 m flume and a still water depth of h = 1.0 m, a 1:5 fore reef and a dry reef flat, a Manning coefficient n = 0.012 is used to approximate the surface roughness. In the experiment, the wave starts to skew to the front as it propagates across the toe of the slope at x = 17 m, and gradually the wave surges over the flat reef undergoing a transition from subcritical flow to supercritical flow around $t\sqrt{g/h}=56$ after the wave surges onto the dry reef, it forms as sheet flow, meanwhile, the reef edge exposed because the rarefaction falls below the initial water level (Roeber et al., 2010). Figure 6 shows the comparison between the measured and simulated wave profiles as the solitary wave propagates across the flume, it can be seen that the numerical model correctly predict the wave surge, flow transition process, sheet flow, wave front and even the offshore rarefaction.

CONCLUSIONS

In this paper, a one-dimensional non-hydrostatic wave model for wave propagation, breaking and run-up has been developed based on the work of Stelling and Duinmeijer (2003). The model solves the depth-integrated, non-conservation form of shallow water equations with extra non-hydrostatic pressure terms. As the existing formulation can properly simulate hydraulic jump with a conservation scheme and handle the moving boundary with a simple and efficient wetting and drying algorithm, the

newly developed non-hydrostatic module enables the model for dynamic wave motion simulation. Analytical solution and experimental data have been used to verify and validate the model, the results show that the developed wave model is suitable for nearshore phenomena simulation, and it is able to handle nonlinear dispersive waves propagation, wave shoaling, breaking and run-up to a certain degree.

ACKNOWLEDGEMENT

REFERENCES

Ai, C., Jin, S., 2012. A multi-layer non-hydrostatic model for wave breaking and run-up. Coastal Engineering 62, 1–8.

Ai, C., Jin, S., Lv, B., 2011. A new fully non-hydrostatic 3D free surface flow model for water wave motions. International Journal for Numerical Methods in Fluids 66, 1354–1370.

Bai, Y., Cheung, K. F., 2011. Depth-integrated free-surface flow with a two-layer non-hydrostatic formulation. International Journal for Numerical Methods in Fluids. doi: 10.1002/fld.2566

Bai, Y., Cheung, K. F., 2012. Depth-integrated free-surface flow with parameterized non-hydrostatic pressure. International Journal for Numerical Methods in Fluids. doi: 10.1002/fld.3664

Beji S, Battjes J.A., 1993. Experimental investigation of wave propagation over a bar. Coastal Engineering 19, 151–162.

Casulli V, Stelling G.S., 1998. Numerical simulation of 3D quasi-hydrostatic, free-surface flows. Journal of Hydraulic Engineering 124, 678–686.

Cui, H., Pietrzak, J.D., Stelling, G.S., 2012. Improved efficiency of a non-hydrostatic, unstructured grid, finite volume model. Ocean Modelling 54-55, 55–67.

Luth HR, Klopman G, Kitou N., 1994. Project 13G: kinematics of waves breaking partially on an offshore bar; LDV measurements for waves with and without a net onshore current. Technical Report H1573, Delft Hydraulics.

Ma, G., Shi, F., Kirby, J.T., 2012. Shock-capturing non-hydrostatic model for fully dispersive surface wave processes. Ocean Modelling 43-44, 22–35.

Roeber, V., Cheung, K.F., Kobayashi, M.H., 2010. Shock-capturing Boussinesq-type model for near-shore wave processes. Coastal Engineering 57, 407–423.

Sorensen, R.M., 2006. Basic Coastal Engineering (3rd edition), Springer,Berlin.

Stansby , P. K., Zhou, J. G., 1998. Shallow-water flow solver with non-hydrostatic pressure: 2D vertical plane problems. International Journal for Numerical Methods in Fluids 28, 541–563.

Stelling, G.S., and Duinmeijer, S.P.A., 2003. A staggered conservative scheme for every Froude number in rapidly varied shallow water flows. International Journal for Numerical Methods in Fluids 43, 1329-1354.

Stelling, G.S., and Zijlema, M., 2003. An accurate and efficient finite-difference algorithm for non-hydrostatic free-surface flow with application to wave propagation. International Journal for Numerical Methods in Fluids 43, 1-23.

Titov, V. V., Synolakis, C. E., 1995. Modeling of breaking and nonbreaking long-wave evolution and runup using VTCS-2. Journal of waterway, port, coastal, and ocean engineering 121, 308-316.

Walters R. A., 2005. A semi-implicit finite element model for non-hydrostatic (dispersive) surface waves. International Journal for Numerical Methods in Fluids 49, 721–737.

Yamazaki Y, Kowalik Z, Cheung K.F., 2008. Depth-integrated, non-hydrostatic model for wave breaking and run-up. International Journal for Numerical Methods in Fluids 61, 473–497.

Zijlema M, Stelling G.S., 2008. Efficient computation of surf zone waves using the nonlinear shallow water equations with non-hydrostatic pressure. Coastal Engineering 55, 780–790.

Zijlema, M., Stelling, G.S., Smit, P., 2011. SWASH: an operational public domain code for simulating wave fields and rapidly varied flows in coastal waters. Coastal Engineering 58, 992-1012.

Zijlema, M. and Stelling, G.S., 2005. Further experiences with computing non-hydrostatic free-surface flows involving water waves. International Journal for Numerical Methods in Fluids 48, 169-197.

A Shallow-Water Equation Based One-Dimensional Dynamic Wave Model with Non-Hydrostatic Pressure
Wei, Jia

Figure 1. Computational domain with free surface and bed elevation.
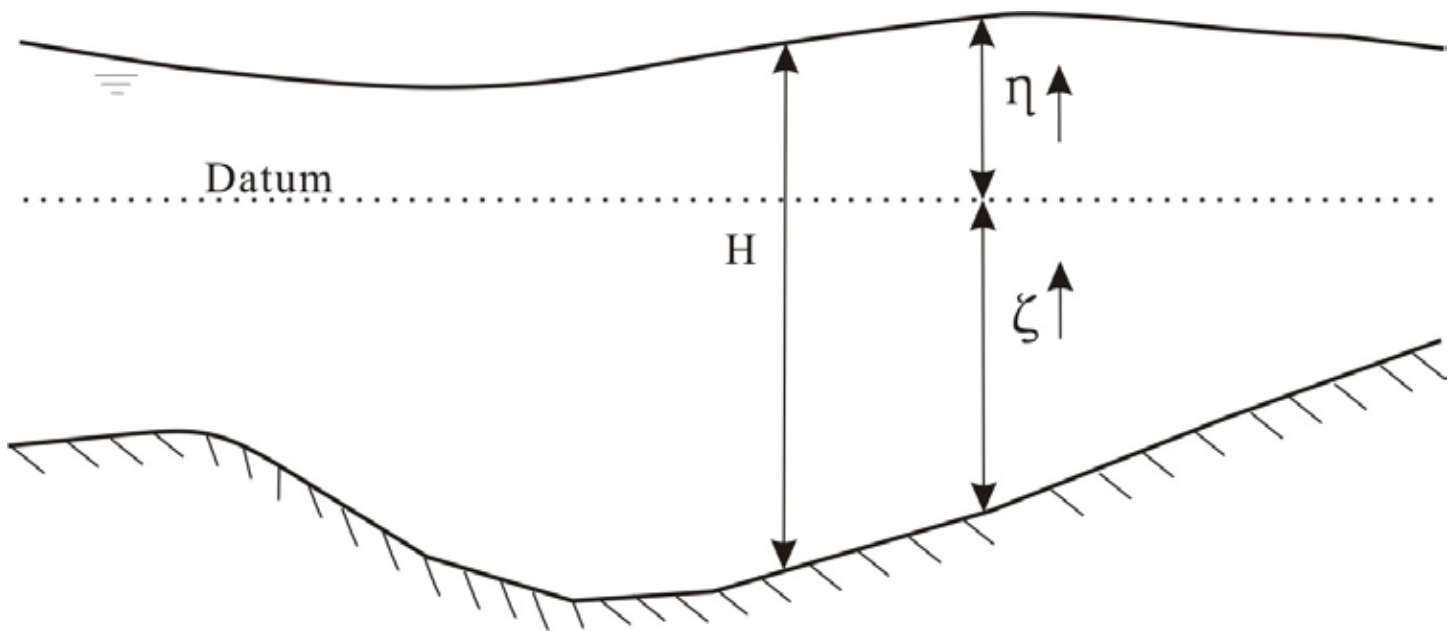

Figure 2. Solitary wave propagation along a channel at different time steps.
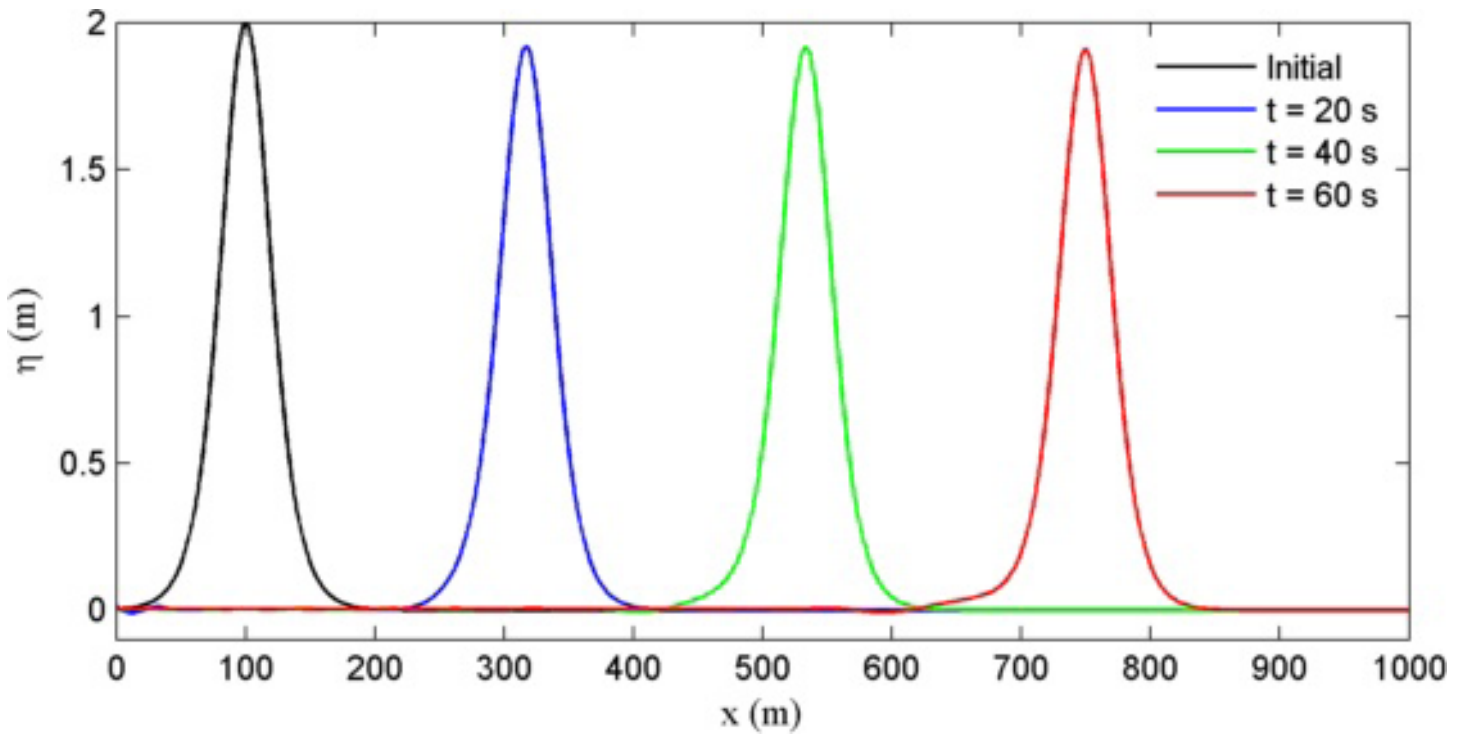
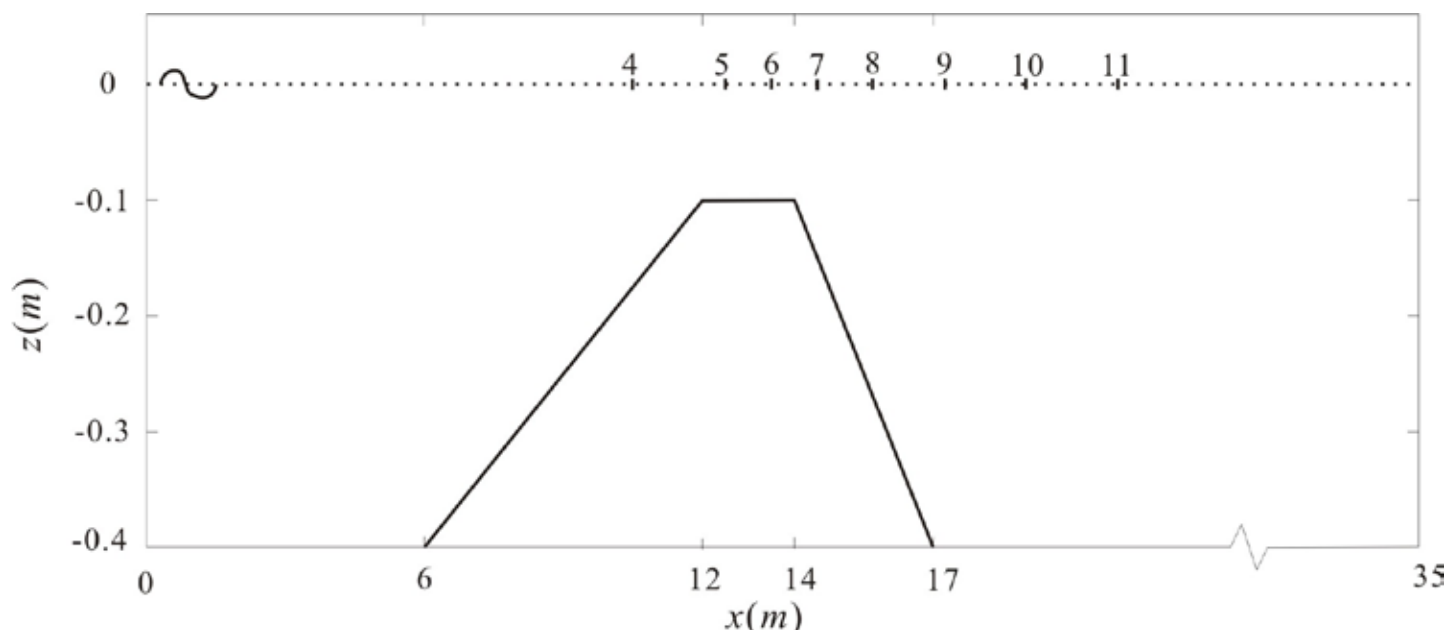**Figure 3. Numerical model setup of waves propagation over a submerged bar.**

Figure 4. Comparison of simulated and measured free surface elevations at several wave gauges. Numerical results (solid lines), experimental data (circles).
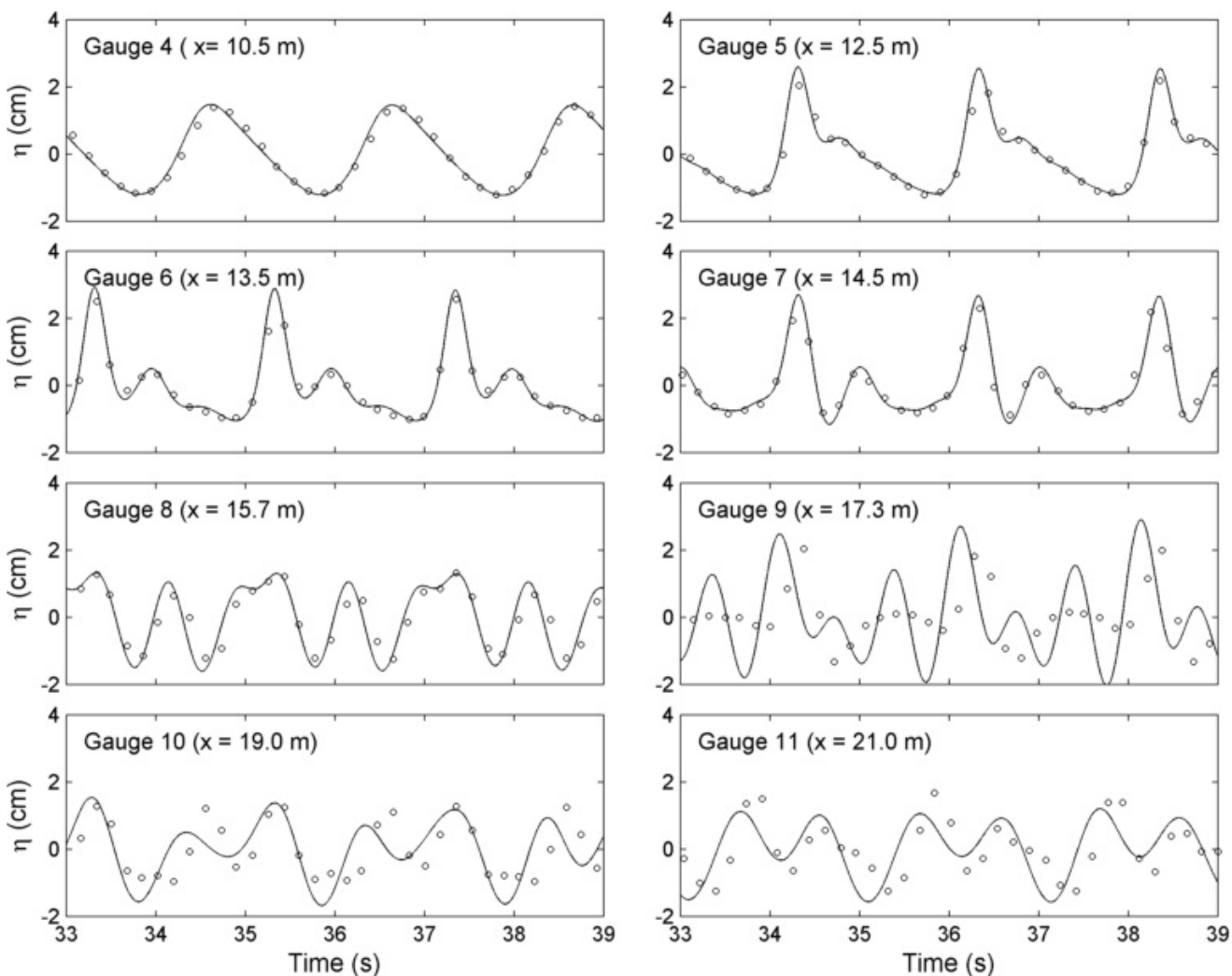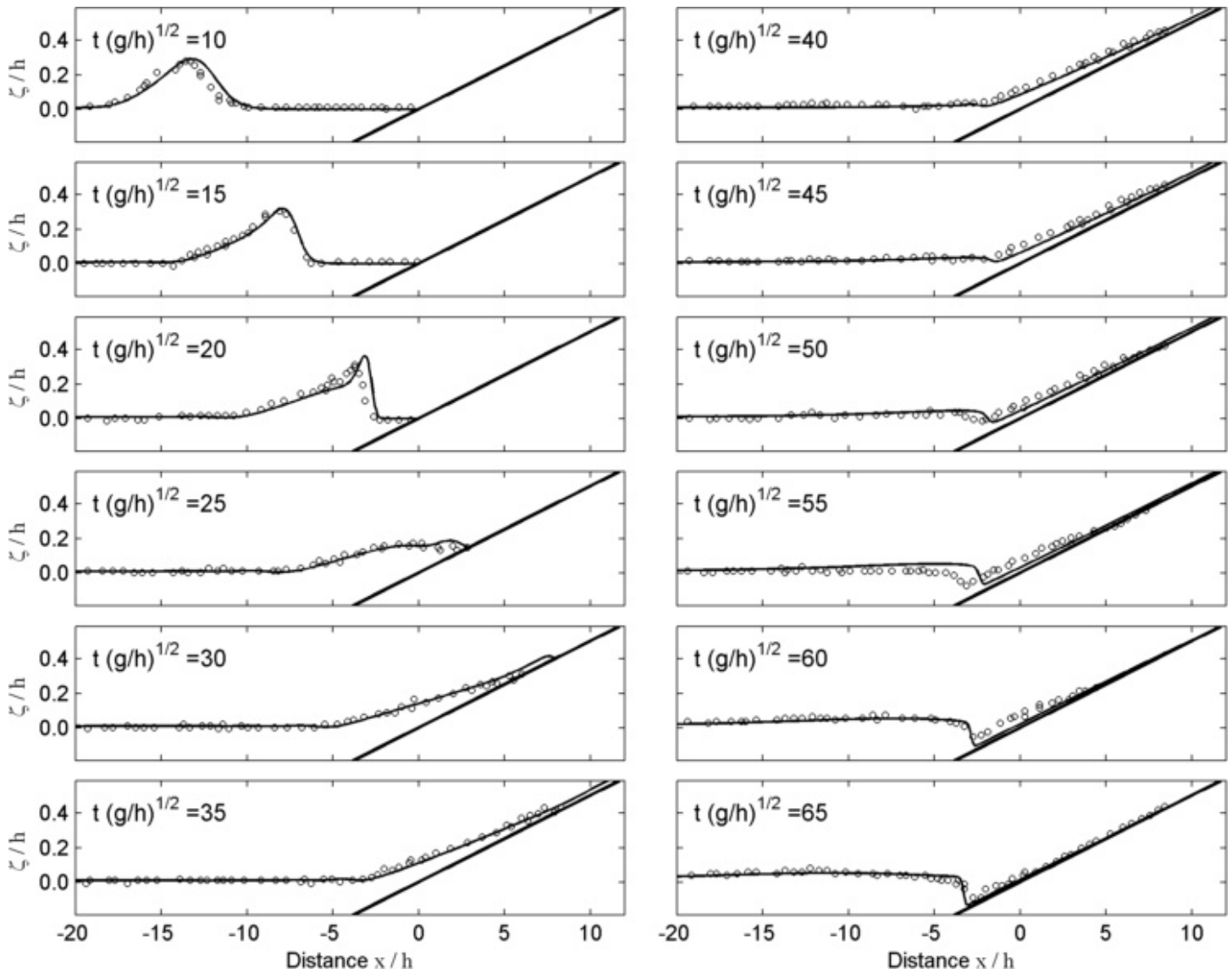
Figure 5. Surface profiles of a solitary wave run-up on a 1:19:85 plane beach. Numerical results (solid lines), experimental data (circles).

Figure 6. Surface profiles of a solitary wave propagation over a fringing reef. Numerical results (solid lines), experimental data (circles).